**AFRL-RV-PS-**
**TP-2014-0004**

**AFRL-RV-PS-**
**TP-2014-0004**

# DIRECT COMPARISON OF A SOLAR MORETON WAVE, EUV WAVE AND CME (PREPRINT)

**S. M. White, et al.**

**30 October 2013**

**Technical Paper**




**AIR FORCE RESEARCH LABORATORY**
**Space Vehicles Directorate**
**3550 Aberdeen Ave SE**
**AIR FORCE MATERIEL COMMAND**
**KIRTLAND AIR FORCE BASE, NM 87117-5776**

# REPORT DOCUMENTATION PAGE

*Form Approved*
*OMB No. 0704-0188*



| **1. REPORT DATE** *(DD-MM-YYYY)* | **2. REPORT TYPE** | **3. DATES COVERED** *(From - To)* |
|---|---|---|
| 30-10-2013 | Technical Paper | 31 Jul 2012 to 30 Sep 2013 |

**4. TITLE AND SUBTITLE**
Direct Comparison of a Solar Moreton Wave, EUV Wave and CME (Preprint)

**5a. CONTRACT NUMBER**

**5b. GRANT NUMBER**

**5c. PROGRAM ELEMENT NUMBER**
61102F

**6. AUTHOR(S)**
S. M. White, K. S. Balasubramaniam, and E. W. Cliver

**5d. PROJECT NUMBER**
2301

**5e. TASK NUMBER**
PPM00005402

**5f. WORK UNIT NUMBER**
EF004365

**7. PERFORMING ORGANIZATION NAME(S) AND ADDRESS(ES)**
Air Force Research Laboratory
Space Vehicles Directorate
3550 Aberdeen Avenue SE
Kirtland AFB, NM 87117-5776

**8. PERFORMING ORGANIZATION REPORT NUMBER**
AFRL-RV-PS-TP-2014-0004

**9. SPONSORING / MONITORING AGENCY NAME(S) AND ADDRESS(ES)**

**10. SPONSOR/MONITOR'S ACRONYM(S)**
AFRL/RVBXS

**11. SPONSOR/MONITOR'S REPORT NUMBER(S)**

**12. DISTRIBUTION / AVAILABILITY STATEMENT**

Approved for public release; distribution is unlimited. (377ABW-2013-0909 dtd 06 Nov 2013)

**13. SUPPLEMENTARY NOTES**
To be submitted to Astrophysical Journal, Projected publication date is March 2014, IOP Publishing. Government Purpose Rights.

**14. ABSTRACT**
On 2011 February 14, the ISOON telescope at the National Solar Observatory at Sacramento Peak recorded a Moreton wave associated with a 1B flare (GOES class M2 with a 1–8 Å maximum at 17:26 UT). The solar event was well observed by the STEREO spacecraft (both in quadrature from Earth) and SDO. The Moreton wave was first observed at 17:25 UT and propagated away from the flare site in a north-easterly direction at a speed of 730 km $s^{-1}$. It displayed a characteristic down–up vertical velocity pattern and lagged slightly (4 x $10^4$ km) behind an EUV wave observed by the Atmospheric Imaging Assembly on SDO to be travelling with essentially the same speed and trajectory. STEREO EUVI and COR1 data indicate that the fast wave was associated with the northward lateral expansion of a coronal mass ejection (CME). The radial CME speed deduced from STEREO A observations was only 580 km $s^{-1}$, but STEREO EUV observations of the low corona indicate an initial lateral speed of 700 km $s^{-1}$ near the time of wave onset, with the coronal portion significantly leading the surface response. A distance vs. time plot of the EUV wave along its main trajectory shows an initial fast bright wave that has a constant speed over 6 x $10^5$ km and reflects off an active region within its angular span, followed by a slower bright wave that becomes stationary.

**15. SUBJECT TERMS**
Sun – Moreton Wave; Sun – Coronal Mass Ejection; Sun – EUV Wave

| **16. SECURITY CLASSIFICATION OF:** | | | **17. LIMITATION OF ABSTRACT** | **18. NUMBER OF PAGES** | **19a. NAME OF RESPONSIBLE PERSON** |
|---|---|---|---|---|---|
| **a. REPORT** | **b. ABSTRACT** | **c. THIS PAGE** | | | E. W. Cliver |
| Unclassified | Unclassified | Unclassified | Unlimited | 22 | **19b. TELEPHONE NUMBER** *(include area code)* |

# Direct Comparison of a Solar MoretonWave, EUV Wave and CME

S. M. White
*Space Vehicles Directorate, Air Force Research Laboratory, Kirtland AFB, NM, 87117, USA*

K. S. Balasubramaniam
*Space Vehicles Directorate, Air Force Research Laboratory, Kirtland AFB, NM, 87117, USA*

E. W. Cliver
*Space Vehicles Directorate, Air Force Research Laboratory, Sunspot, NM, 88349, USA*

## ABSTRACT

On 2011 February 14, the ISOON telescope at the National Solar Observatory at Sacramento Peak recorded a Moreton wave associated with a 1B flare (GOES class M2 with a 1–8 Å maximum at 17:26 UT). The solar event was well observed by the STEREO spacecraft (both in quadrature from Earth) and SDO. The Moreton wave was first observed at 17:25 UT and propagated away from the flare site in a north-easterly direction at a speed of 730 km s−1. It displayed a characteristic down–up vertical velocity pattern and lagged slightly (4 x 104 km) behind an EUV wave observed by the Atmospheric Imaging Assembly on SDO to be travelling with essentially the same speed and trajectory. STEREO EUVI and COR1 data indicate that the fast wave was associated with the northward lateral expansion of a coronal mass ejection (CME). The radial CME speed deduced from STEREO A observations was only 580 km s−1, but STEREO EUV observations of the low corona indicate an initial lateral speed of 700 km s−1 near the time of wave onset, with the coronal portion significantly leading the surface response. A distance vs. time plot of the EUV wave along its main trajectory shows an initial fast bright wave that has a constant speed over 6 x 105 km and reflects off an active region within its angular span, followed by a slower bright wave that becomes stationary.

Key words: Sun – Moreton Waves; Sun – Coronal Mass Ejections; Sun – EUV Waves

## 1. INTRODUCTION

Moreton waves, large-scale Hα waves that propagate away from flare sites with typical speeds 500-1000 km $s^{-1}$ and angular spans 50-100° (Smith & Harvey 1971), were first reported over 50 years ago by Moreton (1960, 1961) and Moreton & Ramsey (1960). Uchida (1968) interpreted Moreton waves as the effect of the "sweeping skirt" of a coronal shock wave on the chromosphere and subsequently (Uchida 1974) linked Moreton waves to solar metric type II radio bursts (Gopalswamy 2000). The discovery of "EIT" waves (Thompson et al. 1999, 2000b) by the Extreme-ultraviolet Imaging Telescope (Delaboudiniére et al. 1995) on SOHO has led to a resurgence of interest in large-scale solar waves. In addition to such waves in Hα, metric radio, and EUV wavelengths, counterparts have been reported during the last decade in soft X-rays (Khan & Aurass 2002; Hudson et al. 2003), He I 10830 Å (Vršnak et al. 2002; Gilbert & Holzer 2004), and microwaves (Warmuth et al. 2004a; White & Thompson 2005). Based on a kinematical analysis, Warmuth et al. (2004a,b) extended Uchida's synthesis to all of the wavelengths at which large-

scale waves are observed. From their analysis showing that large-scale waves exhibited deceleration, profile broadening, and amplitude damping, Warmuth et al. argued that such waves were freely propagating. Alternatively, Zhukov & Auchère (2004) suggested that EIT waves may consist of two separate types: a mode due to magnetic restructuring associated with a coronal mass ejection, and a true wave mode. Support for an eruptive mode view of EIT waves has been presented by several authors (e.g., Delannée & Aulanier 1999; Delannée 2000; Chen et al. 2002, 2005; Harra & Sterling 2003; Attrill et al. 2007, 2009; Delannée et al. 2008; Cohen et al. 2009; Wills-Davey & Attrill 2009; Zhukov et al. 2009; Dai et al. 2010; Yang & Chen 2010; Chen & Wu 2011; Warmuth & Mann 2011). As noted by Balasubramaniam et al. (2010), however, "The view that some EIT waves are 'pseudo-waves' has prompted a reaction - several recent papers based on high-cadence STEREO observations (Long et al. 2008; Veronig et al. 2008; Gopalswamy et al. 2009; Patsourakos & Vourlidas 2009; Patsourakos et al. 2009; Kienreich et al. 2009; Veronig et al. 2010) show that other traveling EIT disturbances definitely are freely propagating MHD waves." The latest studies from STEREO and SDO (Liu et al. 2010; Grechnev et al. 2011; Harra et al. 2011; Ma et al. 2011; Veronig et al. 2011; Zhao et al. 2011; Cheng et al. 2012; Dai et al. 2012; Kumar & Manoharan 2013; Kumar et al. 2013; Li et al. 2012) have presented additional evidence for both propagating "non-wave" EUV disturbances and fast–mode EUV waves, in several cases in the same event. For recent reviews on the nature (wave or non-wave) of propagating EUV disturbances, see Wills-Davey & Attrill (2009), Warmuth (2011), Chen & Fang (2012), Gallagher & Long (2011), Zhukov (2011), and Patsourakos & Vourlidas (2012).

The other outstanding question for large-scale waves - beyond the debate between adherents of the magnetic restructuring and true wave pictures for EIT waves - involves their origin and applies only for the "true wave" picture. Simply put (e.g., Vršnak & Cliver 2008), are such waves the result of a flare explosion (pressure pulse) or are they driven (at least initially) by a coronal mass ejection? Recent evidence based on EUV observations by STEREO, SDO and *Hinode* (Veronig et al. 2008; Liu et al. 2009; Patsourakos & Vourlidas 2009; Patsourakos et al. 2009; Kienreich et al. 2009; Veronig et al. 2010; Liu et al. 2010; Ma et al. 2011; Temmer et al. 2011; Zheng et al. 2011; Bain et al. 2012; Cheng et al. 2012; Dai et al. 2012; Kumar & Manoharan 2013) supports the CME-driver picture, although there is also recent evidence for flare–initiated waves.

Most of the above evidence for CME drivers is based on observations of EUV waves. Because of their rarity, there is relatively little direct evidence that Moreton waves are CME-driven. Narukage et al. (2008) linked each of three separate Moreton waves associated with the same M1 flare to separate filament eruptions but not to separate CMEs (one was reported). From an analytic model of the Moreton wave on 2005 January 17, Temmer et al. (2009) concluded that the wave was driven either by expansion of the flanks of the associated CME or by a flare pressure pulse (piston drivers; Lulić et al. 2013) but not by the CME bow shock (see Vršnak 2005, for a primer on the terminology of large-scale waves). For the Moreton wave on 2003 October 28, Muhr et al. (2010) attributed two wave ignition centers to expansion of the ends of a flux rope, inferred to be the flanks of a CME from the presence of twin EUV dimming regions, rather than to flare heating. Balasubramaniam et al. (2010) argued that the well-defined Moreton wave on 2006 December 6 was driven by the lateral expansion of an erupting arcade (i.e., CME) but their analysis was hampered by the lack of coronagraph observations. All of the above events occurred prior to high-cadence coronagraph observations by STEREO. To date, only one Moreton wave (2011 August 9; Asai et al. 2012) has been reported during the STEREO era, but apparently there was no

STEREO coronagraph coverage for the event and LASCO did not obtain an image until late in the EUV wave observations. The EUV waves associated with this event were observed by SDO. Asai et al. (2012) reported a fast bright EUV wave that was cospatial with the Moreton wave and which persisted as a fast faint wave after the Moreton wave disappeared. These propagating EUV disturbances were identified as fast–mode magnetohydrodynamic (MHD) waves. They also identified a slow bright wave behind the fast waves which stopped propagating on encountering active regions. Asai et al. (2012) tentatively suggested that the bright front might correspond to the flank of a CME. More recently, Shen & Liu (2012) suggested that an EUV dimming region behind the bright front in the 2011 August 9 event might map the CME footprint on the solar surface (e.g., Thompson et al. 2000a).

In this paper we will investigate the origin of the solar Moreton wave of 2011 February 14 and its association with a simultaneous EUV "wave"[1] and a coronal mass ejection. The associated eruptive solar event was well-observed by STEREO (with both spacecraft nearly 90° from the Earth-Sun line) and by SDO. The observations are presented in section 2 and the results are summarized and discussed in section 3.

## 2. OBSERVATIONS

The flares from NOAA AR 11158 in mid-February, 2011, were some of the first major flares of the current solar cycle, including (on Feb. 15) the first X–class flare of the cycle. A number of these flares exhibited dramatic propagating global disturbances in EUV images obtained in wavelength bands dominated by coronal lines with the Solar Dyamics Observatory (SDO) Atmospheric Imaging Assembly (AIA) telescope: for convenience, we will refer to these as "EUV waves". We study the M2 flare on February 14, whose impulsive phase begins at around 17:23:45 UT.

### 2.1. ISOON

The observations of the Moreton wave in this event are Hα centerline and ±0.4 Å images obtained by the prototype ISOON patrol telescope (Neidig et al. 1998) located at the National Solar Observatory (NSO), Sacramento Peak. The ISOON telescope is a 25 cm polar axis refractor. The data consist of photometric quality (<5% uncertainty) images at selected wavelengths in a 2048 x 2048 pixel grid, with a nominal angular resolution of 1.09 arcsec. At present, Hα centerline and off-band images are made every minute (with centerline taken approximately on the minute and red and blue following, in turn, at 3-4 s intervals), a white-light image (WL) every 5 minutes, and an He I 10830 °A image every 10 minutes. For the analysis here we carried out the standard ISOON calibration (normalization for quiet–Sun intensity, correction for atmospheric refraction, and removal of limb darkening, e.g. Kirk et al. 2012), and in addition the images were all corrected for solar rotation so that coordinates correspond to a common time (17:20 UT).

The flare center in AR 11158 is located close to disk center (heliographic coordinates S20W06, 70″ west and 236″ south of apparent disk center). The Moreton wave (i.e., distinct motion of Hα–emitting material) is clearly visible in the sequence of 1–minute Hα centerline images for

[1]For convenience and brevity we will use the term "wave" for the propagating disturbance in the remainder of this paper, recognizing that there is an ongoing debate as to whether these disturbances are true waves.

about 7 minutes from 17:25 until 17:32 UT, but only in an arc of propagation angles centered at about 35◦ east of north. Images at two discrete times are shown in Figure 1 (right panels). An extended region of bright Hα emission surrounds the flare site in the active region, and a feature propagates to the north–east, across the region of disk center and to the east of AR 11159, which was just west of the central meridian in the northern hemisphere.

ISOON Hα images in the red and blue wings (80 mÅ wide at ±0.4 Å) are differenced to make line–of–sight Doppler velocity images. Standard processing of the red and blue images is first carried out, then the images are coaligned and the difference is converted into a line-of-sight velocity (in meters per second) using a calibration table derived by shifting a full Hα line profile though the ISOON passbands. The images use the standard optical convention that red–shifted emission is bright in the velocity images.

Since the disturbance propagates across disk center, the line-of-sight velocity in this event is dominated by vertical motions in the chromosphere, and bright emission in the Doppler images represents down going material. As shown in Figure 2 and discussed further below, the wave was clearly visible in the Doppler velocity images, but the Doppler response lags behind the line center emission.

### 2.2. SDO/AIA

This event was well–observed by the AIA telescope, which makes images in a number of EUV wavelength bands with a typical cadence of 12 seconds at each wavelength (Lemen et al. 2011). A propagating disturbance was visible in most of the coronal EUV bands: here we use the 211 Å images, where it was prominent. The strongest emission line in the 211 Å band is an Fe XIV line, producing a peak response at temperatures in the 2–3 x $10^6$ K range (Boerner et al. 2012). AIA images at times matching those of the ISOON images are shown in the left panels in Fig. 1. The leading edge of the disturbance in the AIA images is marked by a curved white line, which is reproduced for reference in the corresponding Hα images in Fig. 1.

An important question that has been difficult to address previously due to the low cadence of EUV images is the relationship between the EUV and Moreton waves in events in which both are observed. At the normal 12–minute cadence of SOHO/EIT images, a disturbance travelling at 500 km $s^{-1}$ has propagated half a solar radius between successive EUV images, and so spreading and dissipation over such distances makes it difficult to recognize a fast disturbance. For this reason the SOHO/EIT wave catalog is strongly biased towards slower speeds: plane–of–the–sky speeds for 160 events reported by Thompson & Myers (2009) show a broad distribution between 50 and 300 km $s^{-1}$ with a maximum speed of just 420 km $s^{-1}$. By contrast, Moreton waves are more easily detected at faster velocities: the mean speed in a sample of 12 Moreton waves observed at the Hida Observatory is 660 km $s^{-1}$ (Zhang et al. 2011).

It is convenient to address the relationship between Moreton wave and EUV wave speeds for the event discussed here using a time–distance plot, or “J plot”. We derive this plot from a sequence of images from which a common pre–event image has been subtracted (“base difference” images). Starting from a common origin close to the flare center, in each EUV and Ha image we sum the emission in pixels in an arc of angles at a common distance from the center, and plot the resulting profiles as a function of time. Here we use a range ±20◦ on either side of the position angle 35◦east

of north, indicated in the upper left panel of Fig. 1. All pixels within successive distance ranges of 8 original ISOON pixels (6240 km) and 16 original AIA pixels (6880 km) are summed for each distance bin. The resulting time–distance images are then preflare–subtracted to minimize the confusion due to non–propagating features. Figure 2 compares the propagation of the EUV wave at 211 Å (left panel) and the Moreton wave measured in Hα centerline (middle panel) and line–of–sight velocity (right panel, white corresponds to red–shifted material, dark is blue–shifted). A fiducial dashed line corresponding to a speed of 730 km $s^{-1}$, launched from the flare location at 17:22 UT (1 minute before the onset of the flare impulsive phase), is shown in each panel as a reference point.

The speed of 730 km $s^{-1}$ is chosen to match the leading edge of the disturbance seen in the EUV images. In the chosen direction, which is the direction of the fastest and brightest response in both the EUV and Hα images, the leading edge of the disturbance is seen to propagate almost 1 solar radius (in the plane of the sky) with no obvious deceleration. The disturbance is seen in Hα centerline images to possess essentially the same speed, but is visible out to the lesser distance of 3 x $10^5$ km. We have made time–distance 211 Å plots for a range of other position angles around the flare site, and they show the presence of the wave roughly out to ± 90° to either side of PA 35° east of north, but with the speed of the leading edge (at least in the plane of the sky) diminishing as you move away from 35°. These plots also indicate that there is no sign of a propagating disturbance to the south of the flare site.

However, comparison of the Hα centerline and Doppler images clearly does show a difference: the vertical response of the atmosphere is delayed relative to the increase in brightness in the line center, with the first response being a downwards motion of the chromosphere followed by an upwards rebound. The Doppler signature can clearly be seen out as far as 3 x $10^5$ km from the flare site. Net vertical velocities, averaged over the arcs used to make the time–distance plots, are of order ±0.4 km $s^{-1}$. The initial delay of the downwards motion relative to the bright centerline emission is around 1 minute (the time resolution of the ISOON images), and the delay in the upwards rebound relative to the initial downwards motion is 1–2 minutes These features can be seen in Figure 3, which shows the intensity profiles at 4 distinct times for 211 Å, Hα centerline and Hα Doppler velocity. The times shown correspond to the times of the ISOON images, since the cadence of AIA is much higher than that of ISOON (in Fig. 2 the ISOON data are interpolated to the AIA time resolution). Fig. 2 gives the impression that the Hα emission is more delayed relative to the reference 730 km $s^{-1}$ line than is the EUV emission, but one could question whether this is a signal–to–noise effect, since fainter emission in Hα images ahead of the brightest features is harder to see in Hα than in the EUV images due to the lower signal–to–noise in Hα. However, Fig. 3 clearly indicates that the brightest 211 Å emission leads the brightest Hα emission (this is particularly clear at 17:29 UT - the red lines), and that cannot be a signal–to–noise issue. Fig. 3 also suggests that the EUV response can increase with distance from the flare site, and the Hα Doppler response has roughly the same magnitude (larger for the red–shift than the blue–shift) as long as it is visible.

The 211 Å time–distance plot shows several other prominent features apart from the fast leading edge. The horizontal length of bright features behind the leading edge indicate how long the corona remains bright after the initial excitation, and this amounts to almost 10 minutes in some cases, particularly at distances beyond 300000 km. The bright chromospheric response seen in the

Hα centerline does not last as long, but again this may be influenced by signal–to–noise issues. The AIA images also show a second distinct propagating disturbance with marked deceleration: this "wave" emerges out of the bright emission near the flare at about 17:28 UT at a distance of order $10^5$ km from the flare and decelerates from an initial speed of 450 km $s^{-1}$ at 17:29 UT down to about 160 km $s^{-1}$ at 17:34 UT and is then roughly stationary after 17:40 UT. Bright EUV emission continues behind this feature for over 10 minutes (time–distance plots derived from a sequence of running-difference images suggest that slower propagating features may be present at these later times.) One can also see downward–curved features coming off the leading edge of the fast EUV wave, notably at a distance of around 250000 km and again near 330000 km: from watching the movie of AIA images, we believe these to be reflections off active region AR 11159, which lies just to the west of the arc used for the time–distance plot with features in the distance range 2.7–3.6 $x10^5$ km from the flare site. Similar reflections have been reported by Gopalswamy et al. (2009) from STEREO data (but see also Attrill 2010) and Li et al. (2012) from AIA data.

An interesting aspect of this event demonstrated in Fig. 2 is that the fast leading edge of the EUV wave is not bright in the cooler 171 Å AIA images dominated by Fe IX: rather, a faint depression of emission can be seen as the leading feature in the sequence of 171 Å images. This behavior of EUV waves in 171 Å images is not uncommon (e.g., Nitta et al. 2013), and was seen in the EUV wave from the X flare the following day (Schrijver et al. 2011). The depression following the leading edge is apparent in the 171 Å "J-plot" in Fig. 2, whereas the slower feature is bright in 171 Å as it is in 211 Å. The AIA images in the hotter bands 193 Å (Fe XII) and 335 Å (Fe XVI) show the same features as the 211 Å (Fe XIV) images.

### 2.3. STEREO EUVI data

We are aided in the analysis of this event by the fact that it occurred at the solar limb as viewed by both STEREO spacecraft. STEREO B was at heliographic longitude 93.7° behind the Earth, STEREO A was 87.0° ahead of the Earth, and the flare occurred roughly 4° west of disk center. Hence it was about 7° onto the disk as seen from STEREO A, and 7° behind the limb from STEREO B. The event was seen both by the Extreme UltraViolet Imager (EUVI) and by the coronagraphs COR1 (field of view 1.3-4.0 $R_\odot$) and COR2 (2–15 $R_\odot$) on both spacecraft. We use EUVI 195 Å images, which are available at a cadence of order 5 minutes; COR1 images at a cadence of 5 minutes from STEREO B and 10 minutes from STEREO A; and COR2 images at a cadence of 15 minutes.

Figure 4 shows the EUVI 195 Å Fe XII difference images of the event at 17:25/17:26 UT (upper panels) and 17:30/17:31 UT (lower panels). To emphasize the similarity between the views of the two STEREO spacecraft on opposite sides of the Sun, we have flipped the STEREO A images east–west to give the same perspective as the STEREO B images. At 17:25 UT, just 1–2 minutes after flare onset, we see a faint expanding loop above the limb together with much brighter low–lying emission extending northwards from the flare site. More of the low–lying emission is visible from STEREO A than from B, consistent with the location of the flare inside the limb from A's perspective but beyond the limb from B's perspective. The faint features above the limb appear identical in the A and B images. By 17:30 UT the images show a dome–shaped feature extending radially outwards from the limb with a height (in the STEREO B images) of order 370″, and extending 415″ to the north of the flare site, with bright and dark features inside the "dome"

indicating motion of coronal material. For the material above the limb the similarity between the STEREO A and B images is striking. The brightest EUV emission at the northern edge of the disturbance is significantly above the limb, not close to the surface where we might expect the largest densities to be present. In the EUVI-B image at 17:31:03 UT, the northern edge of the dome feature is about 3.0 x $10^5$ km from the flare site, corresponding to a speed very close to 700 km $s^{-1}$ if we assume that the disturbance was launched at 17:24:00 UT. The radial height of the dome of 2.7 x $10^5$ km gives an upwards speed of around 630 km $s^{-1}$. Comparison of the STEREO A and B images suggests an uncertainty of 5–10% in these speeds. Veronig et al. (2010) also report the existence of a dome–shaped feature associated with an EUV wave in 195 Å EUVI-B data: their example is more symmetric than is the case here. They argue that the EUV dome is distinct from the CME body in that event, based largely on the argument that the CME should not be bigger than the observed volume of coronal dimming; however, their images comparing the EUV dome with the CME can be interpreted as showing a single structure.

Interestingly, we can see no signs of an EUV wave propagating across the visible disk in either set of EUVI images. If it is confined to low altitudes, the brightest portion of the EUV wave seen from SDO (Fig. 1) should be visible inside the limb from STEREO B's perspective. The 5–minute cadence of the EUVI images is not optimal for identifying a disturbance travelling at 730 km $s^{-1}$, but it is still bright at 17:30 UT in the AIA images. Its absence against the disk in the STEREO B images suggests that the disturbance seen by AIA is indeed well above the solar photosphere, consistent with the interpretation that the dome seen in Fig. 4 is responsible for the propagating feature in EUV images.

### 2.4. STEREO coronagraph images

Consistent with the expanding dome feature seen in the EUVI images, a coronal mass ejection was present in this event but it has some unusual properties. This is reflected in the conflicting reports in the various CME catalogs: the CDAW LASCO catalog reports a CME with a speed of 326 km $s^{-1}$ propagating 45° north of the ecliptic; the SEEDS LASCO catalog has a speed of 309 km $s^{-1}$ at 32° north; the SEEDS STEREO A COR2 catalog has a speed of 349 km $s^{-1}$; the SEEDS STEREO B COR2 catalog has a speed of 386 km $s^{-1}$; the CACTus LASCO catalog has 241 km $s^{-1}$ at 29° north; the CACTus STEREO A COR2 catalog does not report an event; the CACTus STEREO B COR2 catalog reports two events, one at 347 km $s^{-1}$ 7° north and one at 676 km $s^{-1}$, 18° north; and the STEREO team COR1 catalog reports a "fast and bright eruption" from both satellites.

Figure 5 shows difference images from the coronagraphs on STEREO A and B that help to explain this confusion. To create optimal images, we have embedded the STEREO B COR1 (which has better cadence than STEREO A COR1) images within the (east–west flipped) STEREO A COR2 (which are less occulted than STEREO B COR2) images, taking advantage of the fact that (as seen in Fig. 4) the 180° separation of the satellites results in essentially identical images. Prior to the flare (upper left panel), a set of loops is already slowly expanding north of the equator, possibly associated with AR 11159. At 17:39 UT the CME from the M2 flare is clearly visible as a bright feature in the COR1 image, centered south of the expanding loops and consistent with an origin south of the equator in AR 11158. The CME can clearly be distinguished from the northern loops in subsequent COR1 frames at 17:40 and 17:45 UT, but by 17:50 UT the expanding loops

and the CME appear to have merged into a single expanding feature straddling the equator. Thus by the time the CME reaches the COR2 field of view, it has merged with the northern loops and slowed considerably from its initial speed in COR1. The STEREO COR2 and LASCO C2 images of the event accordingly show a fairly slow unimpressive CME.

The radially–outwards speed of the CME when first seen in COR1 is of order 580 km $s^{-1}$. In Figure 6 we compare the motion of the disturbance in this event using a number of diagnostics. Purple squares represent the height of the leading edge of the CME above the limb in the three COR1 images in which it can clearly be identified, and a fit to these three points yields 580 km $s^{-1}$. The red asterisks show the outer height of the disturbance seen in the COR2 images: before 17:50 UT this height represents the expanding loops north of the flare site, and from 17:55 onwards it represents the merged loop–CME structure. The outwards motion in the COR2 images is closer to the 300 km $s^{-1}$ value reported in the CME catalogs. Blue diamonds show the height above the limb of the "dome" in the EUVI A and B images (Fig 4), while the green line is the 730 km $s^{-1}$ (transverse across the disk, not radially outwards above the limb) motion of the EUV wave in the AIA images.

## 3. DISCUSSION

It is clear from Figs. 1 & 2 that the Moreton wave observed in the chromospheric Hα line and the fast EUV wave observed in coronal lines by AIA are associated: in this event, with the convenient geometry that motion occurs across the center of the disk, they have essentially the same trajectory and the same speed. More detailed comparison is limited by the lower signal–to–noise of the Hα images compared to the EUV images from above the atmosphere, but it also appears (Fig. 3) that the Hα response lags slightly behind the EUV disturbance. The STEREO EUVI images, viewing the event from side–on at the limb, indicate that the leading edge seen from above in the AIA images is the outer edge of an expanding partial dome. This dome is not quite circular: the distance from the flare site to the northern edge of the dome appears to be a little larger than the radial height of the dome above the flare site, but the difference is small.

The presence of the Hα Moreton wave delayed slightly behind the coronal response and the observed vertical velocity response in which initially the Hα–emitting layer moves downwards, followed by an upwards rebound, appear to be consistent with a picture in which a pressure increase in the corona acts to compress the chromosphere from above, enhancing the density and driving the top of the chromosphere downwards. The vertical velocities induced, averaged over the arc used to make Fig. 2, are of order 0.4 km $s^{-1}$. Ideally we could use these measurements to estimate the pressure pulse, but this is a difficult calculation due to the complexity of the formation of the Hα line, uncertainty about the height of emission in Moreton waves (e.g., Balasubramaniam et al. 2007) and the need to know the atmospheric structure in order to calculate the response to a given pressure impulse. Such a calculation is beyond the scope of this paper.

The horizontal extent of the bright features in the J plots (Fig. 2, but note that the apparent duration of weak signal–to–noise features depends greatly on the method of background subtraction) reflects the amount of time that a feature remains bright after the passage of the leading edge. In the picture in which the enhanced emission in the corona results from an increase in density due to compression, the duration of bright emission is controlled either by cooling of the

gas out of the temperature range to which a given AIA band is sensitive, or to relaxation of the density enhancement back to the original state. As an example, the bright material at a distance of order 4 x $10^5$ km in Fig. 2 (left panel) has a duration of about 10 minutes. The typical intensity of the brightening is roughly 10 DN pixel$^{-1}$ s$^{-1}$ (averaged over the 40° wide arc at this distance). Assuming a response appropriate to the peak of the 211 °A temperature curve at 2 x $10^6$ K of order 1.5 x $10^{-25}$ DN pixel$^{-1}$ s$^{-1}$ cm$^{-5}$ (Boerner et al. 2012, but using version 4 of the AIA responses released inFebruary 2013), the corresponding column emission measure is 6 x $10^{25}$ cm$^5$. To convert this into a mean density we need to assume a thickness for the emitting layer: from the EUVI images in Fig. 4, $10^{10}$ cm (140″) is a plausible (but highly uncertain) estimate, giving roughly $10^8$ cm$^{-3}$ for the average density of the additional coronal material at 2 x $10^6$ K produced by the passage of the EUV wave. Such a low density is consistent with the argument that the leading edge of the EUV wave is actually about 100″ above the solar surface at this time (Fig. 4). The radiative cooling time at this density and a temperature of 2 MK, assuming a cooling law of $\tau_R = 130.T^{5/3}/n$ (e.g., Aschwanden & Terradas 2008), is of order 50000 seconds, which is much longer than the observed duration. Thus, if these estimates are correct, the duration of bright emission after the passage of the disturbance does not require additional heat input; shorter loss times can be explained by the effects of conduction and faster radiative loss in localized density enhancements.

A Type II radio burst, usually taken to be indicative of the presence of a shock, is seen as early as 17:28 UT (at 200 MHz). There are no imaging observations to show where the burst occurs in relation to the eruption. This early in the flare, the outer edge of the CME is at a height of less than 0.4 R$_\odot$ (Fig. 6).

We noted the presence of two quite bright propagating disturbances in the AIA 211 Å J plot (Fig. 2), one significantly slower than the other. One interpretation of such a double structure is that the fast disturbance is a fast–mode MHD wave and the slower disturbance is associated with the CME. However, the EUVI and COR1 data suggest that the faster wave in this event is coincident with the leading edge of the mass ejection. Inspection of the AIA images suggest that the slower structure, which becomes stationary before it reaches AR 11159, consists of slower–moving material that leaves the flare site later than the fast disturbance and becomes becalmed in the region between AR 11158 and 11159 when it encounters material associated with the reflections from AR 11159. The STEREO–B EUVI image at 17:35 shows bright material elevated at heights of up to 2.5 x $10^5$ km above the limb in the volume between the two active regions, suggesting either that the reflected material has significant vertical motion or the interaction of the reflected material and the slower flare material results in vertical motion.

## 4. CONCLUSIONS

We report on a solar eruptive flare in which an Hα Moreton wave, EUV wave and CME are all well observed simultaneously, and in the case of the EUV wave and CME, from three directions. The leading EUV wave has a nearly constant speed of 730 km s$^{-1}$ over a large distance; for much of its motion, the Hα Moreton wave has the same speed but the brightest Hα emission appears to lag behind the brightest EUV emission. By contrast, the CME expands radially at about 580 km s$^{-1}$ early in the event, and then appears to decelerate rapidly and eventually dissipate when it encounters an adjacent slowly expanding loop system at a height of order 2 R$_\odot$. EUVobservations from the STEREO spacecraft, for which the event is at the limb, show a dome–

shaped feature 5 minutes after flare onset whose bright northern leading edge appears to match the leading edge of the EUV wave. The northern edge of this dome is well (~ 100″) above the surface. Velocity measurements with the Hα line data from ISOON clearly show that the chromosphere is first pushed downwards as the wave passes, and then rebounds upwards, as if a pressure pulse has passed by. The delay of the Hα response and the velocity behavior of the chromosphere are consistent with the region inside the dome exerting additional pressure on the solar atmosphere, compressing the corona to produce additional EUV emission, and initially pushing down on the chromosphere to produce the red–shifted Moreton wave. Harra et al. (2011) and Veronig et al. (2011) report velocity measurements in coronal lines from an EUV wave from the same active region 2 days later, in which they found that coronal material also initially moves downwards as the wave passes and then rebounds upwards. The data for our event are consistent with the EUV dome being identical with the CME low in the solar atmosphere: the difference between the northward velocity of the EUV wave and the radial velocity of the CME implies that the CME dome expands faster laterally than it does radially in the early portion of the event. However, the clear presence of propagating EUV features reflected off active regions indicates that some component of the EUV wave has fast–mode MHD wave characteristics.

A second slower (~ 400 km $s^{-1}$) propagating disturbance that decelerates at a distance of 2 x $10^5$ km from the flare site is also seen in the EUV images, but not in the Hα data. A common interpretation of the presence of two EUV wave features is that the first is a fast–mode wave launched by the CME, while the second slower feature represents the CME itself. That picture is not consistent with this event: the slower second EUV feature lags well behind the projected leading edge of the CME. The visual appearance of the AIA images suggests that the slower feature represents actual motion of material outwards from the flare site: Schrijver et al. (2011) argued that the EUV wave from the X2 flare 6 hours later is initiated by the expansion of a set of loops rooted in the active region. As in that case, the fast wave in this event appears to detach itself from the moving material early in the expansion, in this case at about 17:26 UT at a distance of order 90000 km from the flare site. In our event, as in the Feb. 15 X flare, the contrast between the appearance of the EUV wave in the 171 Å Fe IX and 211 Å Fe XIV channels is noteworthy: in 171 Å, no bright leading edge is seen, but a faint dimming follows the passage of the fast wave in 171 Å while in 211 Å the same region is brighter than before the wave passage. We speculate that this is consistent with at least some of the cool material present in the quiet–Sun corona before the passage of the wave being heated out of the Fe IX temperature range and into the Fe XII–XVI (195, 211 & 335 Å) range by compression from the disturbance, as suggested by Wills-Davey & Thompson (1999) and further quantified by Schrijver et al. (2011); see also the survey by Nitta et al. (2013).

We acknowledge support from AFOSR Task 2301RDA1. The National Solar Observatory (NSO) is operated by the Association of Universities for Research in Astronomy under cooperative agreement with the National Science Foundation. SOHO is a project of international cooperation between ESA and NASA. This research has made use of NASAs Astrophysics Data System Bibliographic Services. We thank the STEREO and SDO teams for their open data policy.

## REFERENCES


Asai, A., Ishii, T. T., Isobe, H., Kitai, R., Ichimoto, K., UeNo, S., Nagata, S., Morita, S., Nishida, K., Shiota, D., Oi, A., Akioka, M., & Shibata, K. 2012, Astrophys. J. Letters, 745, L18

Aschwanden, M. J. & Terradas, J. 2008, Astrophys. J. Letters, 686, L127

Attrill, G. D. R. 2010, Astrophys. J., 718, 494

Attrill, G. D. R., Engell, A. J., Wills-Davey, M. J., Grigis, P., & Testa, P. 2009, Astrophys. J., 704, 1296

Attrill, G. D. R., Harra, L. K., van Driel-Gesztelyi, L., & Démoulin, P. 2007, Astrophys. J. Letters, 656, L101

Bain, H. M., Krucker, S., Glesener, L., & Lin, R. P. 2012, Astrophys. J., 750, 44

Balasubramaniam, K. S., Cliver, E. W., Pevtsov, A., Temmer, M., Henry, T. W., Hudson, H. S., Imada, S., Ling, A. G., Moore, R. L., Muhr, N., Neidig, D. F., Petrie, G. J. D., Veronig, A. M., Vršnak, B., & White, S. M. 2010, Astrophys. J., 723, 587

Balasubramaniam, K. S., Pevtsov, A. A., & Neidig, D. F. 2007, Astrophys. J., 658, 1372

Boerner, P., Edwards, C., Lemen, J., Rausch, A., Schrijver, C., Shine, R., Shing, L., Stern, R., Tarbell, T., Title, A., Wolfson, C. J., Soufli, R., Spiller, E., Gullikson, E., McKenzie, D., Windt, D., Golub, L., Podgorski, W., Testa, P., & Weber, M. 2012, Solar Phys., 275, 41

Chen, P. F. & Fang, C. 2012, Bull. Astron. Soc. India

Chen, P. F., Fang, C., & Shibata, K. 2005, Astrophys. J., 622, 1202

Chen, P. F., Wu, S. T., Shibata, K., & Fang, C. 2002, Astrophys. J. Letters, 572, L99

Chen, P. F. & Wu, Y. 2011, Astrophys. J. Letters

Cheng, X., Zhang, J., Olmedo, O., Vourlidas, A., Ding, M. D., & Liu, Y. 2012, Astrophys. J. Letters, 745, L5

Cohen, O., Attrill, G. D. R., Manchester, IV,W. B., &Wills-Davey, M. J. 2009, Astrophys. J., 705, 587

Dai, Y., Auchère, F., Vial, J.-C., Tang, Y. H., & Zong, W. G. 2010, Astrophys. J., 708, 913

Dai, Y., Ding, M. D., Chen, P. F., & Zhang, J. 2012, Astrophys. J., 759, 55

Delaboudinière, J.-P., Artzner, G., Brunaud, J., Gabriel, A., Hochedez, J. F., Millier, F., Song, X. Y., Au, B., Dere, K. P., Howard, R. A., Kreplin, R., Michels, D. J., Moses, J. D., Defise, J. M., Jamar, C., Rochus, P., Chauvineau, J. P., Marioge, J. P., Catura, R. C., Lemen, J. R., Shing, L., Stern, R. A., Gurman, J. B., Neupert, W. M., Maucherat, A., Clette, F., Cugnon, P., & Van Dessel, E. L. 1995, Solar Phys., 162, 291

Delannée, C. 2000, Astrophys. J., 545, 512

Delannée, C. & Aulanier, G. 1999, Solar Phys., 190, 107

Delannée, C., T¨or¨ok, T., Aulanier, G., & Hochedez, J.-F. 2008, Solar Phys., 247, 123

Gallagher, P. T. & Long, D. M. 2011, Space Sci. Revs., 158, 365

Gilbert, H. R. & Holzer, T. E. 2004, Astrophys. J., 610, 572

Gopalswamy, N. 2000, in Radio Astronomy at Long Wavelengths, ed. R. G. Stone, K. W. Weiler, M. L. Goldstein, & J.-L. Bougeret (Washington and DC: American Geophysical Union), 123

Gopalswamy, N., Yashiro, S., Temmer, M., Davila, J., Thompson, W. T., Jones, S., McAteer, R. T. J., Wuelser, J.-P., Freeland, S., & Howard, R. A. 2009, Astrophys. J. Letters, 691, L123

Grechnev, V. V., Afanasyev, A. N., Uralov, A. M., Chertok, I. M., Eselevich, M. V., Eselevich, V. G., Rudenko, G. V., & Kubo, Y. 2011, Solar Phys., 273, 461

Harra, L. K. & Sterling, A. C. 2003, Astrophys. J., 587, 429
Harra, L. K., Sterling, A. C., G¨om¨ory, P., & Veronig, A. 2011, Astrophys. J. Letters, 737, L4
Hudson, H. S., Khan, J. I., Lemen, J. R., Nitta, N. V., & Uchida, Y. 2003, Solar Phys., 212, 121
Khan, J. I. & Aurass, H. 2002, Astron. Astrophys., 383, 1018
Kienreich, I. W., Temmer, M., & Veronig, A. M. 2009, Astrophys. J. Letters, 703, L118
Kirk, M. S., Balasubramaniam, K. S., Jackiewicz, J., McNamara, B. J., & McAteer, R. T. J. 2012, Solar Phys., in press
Kumar, P., Cho, K.-S., Chen, P. F., Bong, S.-C., & Park, S.-H. 2013, Solar Phys., 282, 523
Kumar, P. & Manoharan, P. K. 2013, Astron. Astrophys., 553, A109
Lemen, J. R., Title, A. M., Akin, D. J., Boerner, P. F., Chou, C., Drake, J. F., Duncan, D. W., Edwards, C. G., Friedlaender, F. M., Heyman, G. F., Hurlburt, N. E., Katz, N. L., Kushner, G. D., Levay, M., Lindgren, R. W., Mathur, D. P., McFeaters, E. L., Mitchell, S., Rehse, R. A., Schrijver, C. J., Springer, L. A., Stern, R. A., Tarbell, T. D., Wuelser, J.-P., Wolfson, C. J., Yanari, C., Bookbinder, J. A., Cheimets, P. N., Caldwell, D., Deluca, E. E., Gates, R., Golub, L., Park, S., Podgorski, W. A., Bush, R. I., Scherrer, P. H., Gummin, M. A., Smith, P., Auker, G., Jerram, P., Pool, P., Soufli, R., Windt, D. L., Beardsley, S., Clapp, M., Lang, J., & Waltham, N. 2011, Solar Phys., 275, 17
Li, T., Zhang, J., Yang, S., & Liu, W. 2012, Astrophys. J., 746, 13
Liu, W., Nitta, N. V., Schrijver, C. J., Title, A. M., & Tarbell, T. D. 2010, Astrophys. J. Letters, 723, L53
Liu, Y., Luhmann, J. G., Bale, S. D., & Lin, R. P. 2009, Astrophys. J. Letters, 691, L151
Long, D. M., Gallagher, P. T., McAteer, R. T. J., & Bloomfield, D. S. 2008, Astrophys. J. Letters, 680, L81
Lulić, S., Vr˘snak, B., Žic, T., Kienreich, I. W., Muhr, N., Temmer, M., & Veronig, A. M. 2013, Solar Phys., 286, 509
Ma, S., Raymond, J. C., Golub, L., Lin, J., Chen, H., Grigis, P., Testa, P., & Long, D. 2011, Astrophys. J., 738, 160
Moreton, G. E. 1960, Astron. J., 65, 494
Moreton, G. E. & Ramsey, H. E. 1960, Publ. Astron. Soc. Pacific, 72, 357
Moreton, G. F. 1961, S&T, 21, 145
Muhr, N., Vršnak, B., Temmer, M., Veronig, A. M., & Magdalenić, J. 2010, Astrophys. J., 708, 1639
Narukage, N., Ishii, T. T., Nagata, S., Ueno, S., Kitai, R., Kurokawa, H., Akioka, M., & Shibata, K. 2008, Astrophys. J. Letters, 684, L45
Neidig, D., Wiborg, P., Confer, M., Haas, B., Dunn, R., Balasubramaniam, K. S., Gullixson, C., Craig, D., Kaufman,M., Hull,W.,McGraw, R., Henry, T., Rentschler, R., Keller, C., Jones, H., Coulter, R., Gregory, S., Schimming, R., & Smaga, B. 1998, in Astronomical Society of the Pacific Conference Series, Vol. 140, Synoptic Solar Physics, ed. K. S. Balasubramaniam, J. Harvey, & D. Rabin, 519
Nitta, N. V., Schrijver, C. J., Title, A. M., & Liu, W. 2013, ArXiv e-prints
Patsourakos, S. & Vourlidas, A. 2009, Astrophys. J. Letters, 700, L182
—. 2012, Solar Phys., 281, 187
Patsourakos, S., Vourlidas, A., Wang, Y. M., Stenborg, G., & Thernisien, A. 2009, Solar Phys., 259, 49
Schrijver, C. J., Aulanier, G., Title, A. M., Pariat, E., & Delannée, C. 2011, Astrophys. J., 738, 167
Shen, Y. & Liu, Y. 2012, Astrophys. J. Letters, 752, L23
Smith, S. F. & Harvey, K. L. 1971, in Astrophysics and Space Science Library, Vol. 27, Physics of

the Solar Corona, ed. C. J. Macris, 156
Temmer, M., Veronig, A. M., Gopalswamy, N., & Yashiro, S. 2011, Solar Phys., 273, 421
Temmer, M., Vršnak, B., Žic, T., & Veronig, A. M. 2009, Astrophys. J., 702, 1343
Thompson, B. J., Cliver, E. W., Nitta, N., Delannée, C., & Delaboudinière, J. P. 2000a, Geophys. Res. Lett., 27, 1431
Thompson, B. J., Gurman, J. B., Neupert, W. M., Newmark, J. S., Delaboudinière, J.-P., St. Cyr, O. C., Stezelberger, S., Dere, K. P., Howard, R. A., & Michels, D. J. 1999, Astrophys. J. Letters, 517, L151
Thompson, B. J. & Myers, D. C. 2009, Astrophys. J. Supp., 183, 225
Thompson, B. J., Reynolds, B., Aurass, H., Gopalswamy, N., Gurman, J. B., Hudson, H. S., Martin, S. F., & St. Cyr, O. C. 2000b, Solar Phys., 193, 161
Uchida, Y. 1968, Solar Phys., 4, 30
—. 1974, Solar Phys., 39, 431
Veronig, A. M., Gomory, P., Kienreich, I. W., Muhr, N., Vršnak, B., Temmer, M., & Warren, H. P. 2011, Astrophys. J. Letters, 743, L10
Veronig, A.M.,Muhr, N., Kienreich, I.W., Temmer, M., & Vršnak, B. 2010, Astrophys. J. Letters, 716, L57
Veronig, A. M., Temmer, M., & Vršnak, B. 2008, Astrophys. J. Letters, 681, L113
Vršnak, B. 2005, EOS Transactions, 86, 112
Vršnak, B. & Cliver, E. W. 2008, Solar Phys., 253, 215
Vršnak, B., Warmuth, A., Brajˇsa, R., & Hanslmeier, A. 2002, Astron. Astrophys., 394, 299
Warmuth, A. 2011, Plasma Physics and Controlled Fusion, 53, 124023
Warmuth, A. & Mann, G. 2011, Astron. Astrophys., 532, A151
Warmuth, A., Vršnak, B.,Magdalenić, J., Hanslmeier, A., & Otruba,W. 2004a, Astron. Astrophys., 418, 1101
—. 2004b, Astron. Astrophys., 418, 1117
White, S. M. & Thompson, B. J. 2005, Astrophys. J. Letters, 620, L63
Wills-Davey, M. J. & Attrill, G. D. R. 2009, Space Sci. Revs., 149, 325
Wills-Davey, M. J. & Thompson, B. J. 1999, Solar Phys., 190, 467
Yang, H. Q. & Chen, P. F. 2010, Solar Phys., 266, 59
Zhang, Y., Kitai, R., Narukage, N., Matsumoto, T., Ueno, S., Shibata, K., & Wang, J. 2011, Publ. Astron. Soc. Japan, 63, 685
Zhao, X. H., Wu, S. T., Wang, A. H., Vourlidas, A., Feng, X. S., & Jiang, C. W. 2011, Astrophys. J., 742, 131
Zheng, R., Jiang, Y., Hong, J., Yang, J., Bi, Y., Yang, L., & Yang, D. 2011, Astrophys. J. Letters, 739, L39
Zhukov, A. N. 2011, Journal of Atmospheric and Solar-Terrestrial Physics, 73, 1096
Zhukov, A. N. & Auchère, F. 2004, Astron. Astrophys., 427, 705
Zhukov, A. N., Rodriguez, L., & de Patoul, J. 2009, Solar Phys., 259, 73

## FIGURES

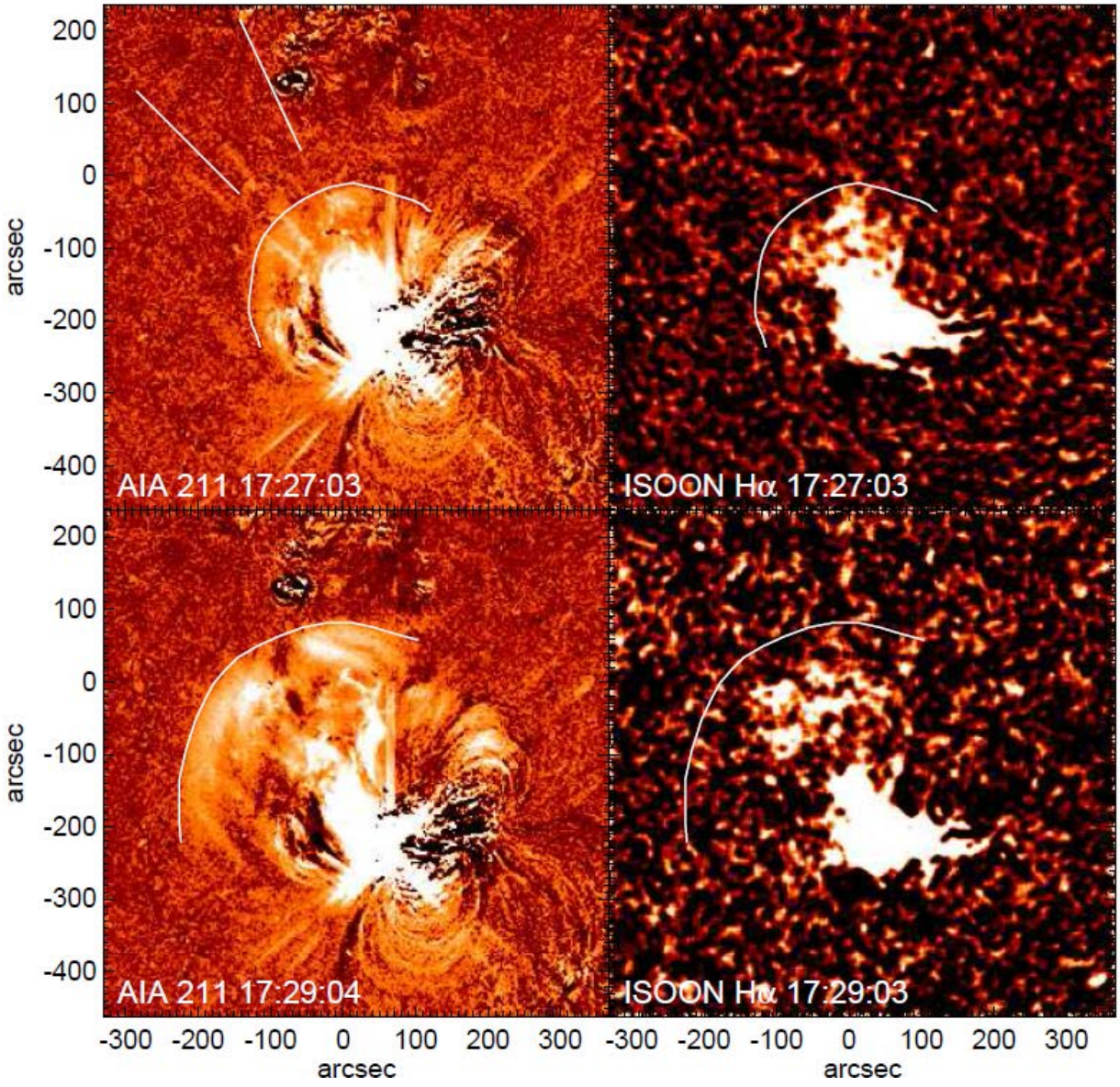


Fig. 1.—Images of the wave from the 2011 February 14 flare in the 211 Å filter of AIA (dominated by Fe XIV, left panels) and in Hα line center from the ISOON telescope (right panels).

In Fig. 1, the images are shown roughly 4 (upper panels) and 6 minutes (lower panels) after the onset of the impulsive phase of the flare, and are differenced against a preflare image. A square–root display is used for the AIA images and a linear display is used for the ISOON images. The southern edge of AR 11159 can be seen at the top of the AIA images. White arcs are drawn on each of the panels at the location of the leading edge of the wave in the AIA 211 Å images at the time of the image. The two straight lines in the upper left panel indicate the range of angles used to measure the speed of the wave.

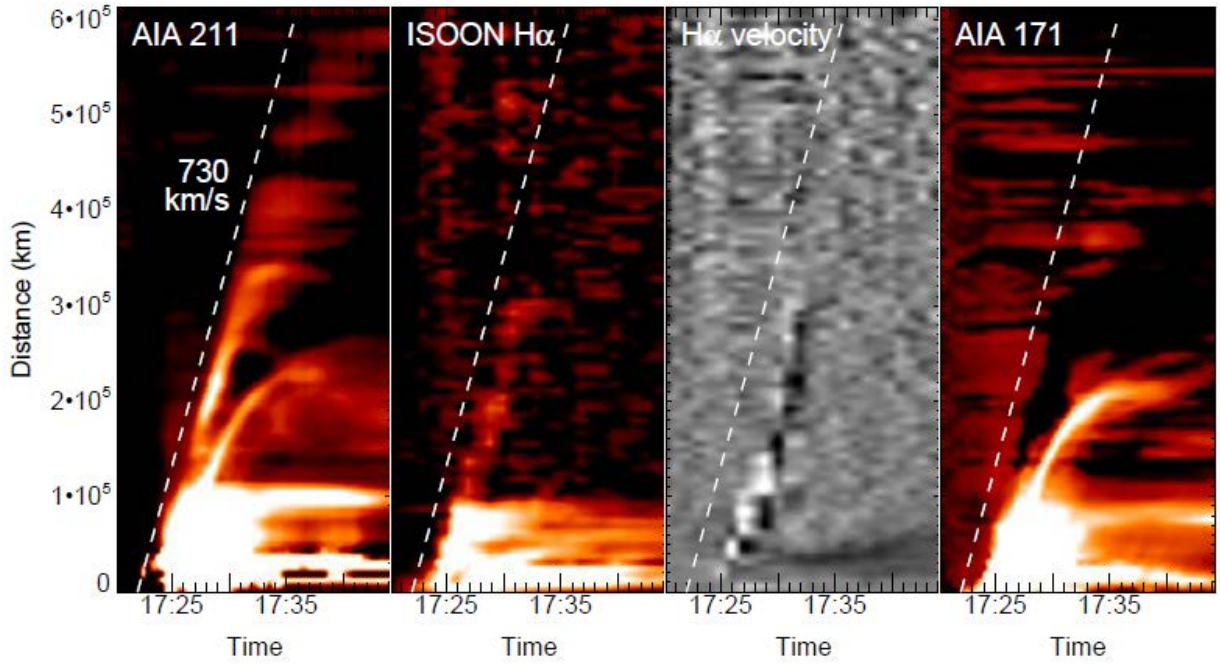


Fig. 2.— Time–distance plots for the wave in the AIA 211 Å images (1st panel), ISOON Hα line center images (2nd), ISOON Hα line–of–sight Doppler images (3rd), and AIA 171 Å images (4th).

In Fig. 2, the plots in each case represent a sum in an arc from 25° east of north to 45° east of north, as shown in Fig. 1. A dashed line corresponding to a disturbance travelling from the flare site at 730 km s−1 is plotted on each panel. In order not to interfere with features in the images, this line is launched at the flare site at 17:22:00 UT, 1 minute before the beginning of the impulsive phase and the launch of the actual wave. The data have been gridded with a uniform time spacing of 24 seconds for plotting. The display range in the 171 Å panel is chosen to emphasize, by contrast with 211 Å, the absence of brightening corresponding to the leading disturbance and the dimming following the disturbance. In panel 3, red–shifted emission is bright and blue–shifted emission dark; the display range is from -0.25 to +0.25 km $s^{-1}$.

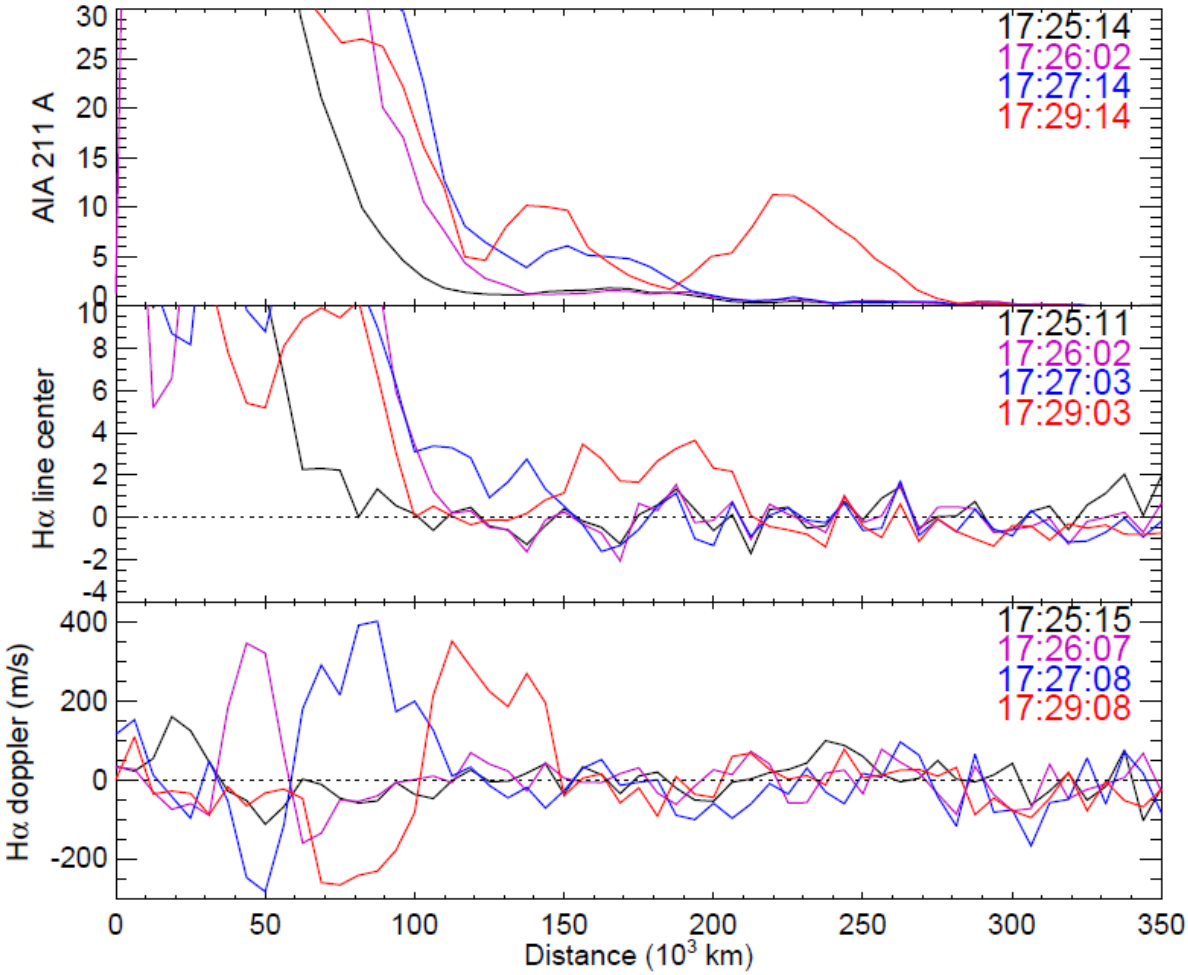


Fig. 3.— Profiles of emission in AIA 211 Å images (top panel), ISOON Hα line center images (middle) and ISOON Hα line–of–sight Doppler images (lower), measured along the arc from 25◦ east of north to 45◦ east of north.

In Fig. 3, all curves are shown at times within 12 seconds of ISOON Hα line center observations. The curves in each panel are shown on the same scale, corrected to a per–unit–area scale, so that absolute trends with time and/or distance can be seen.

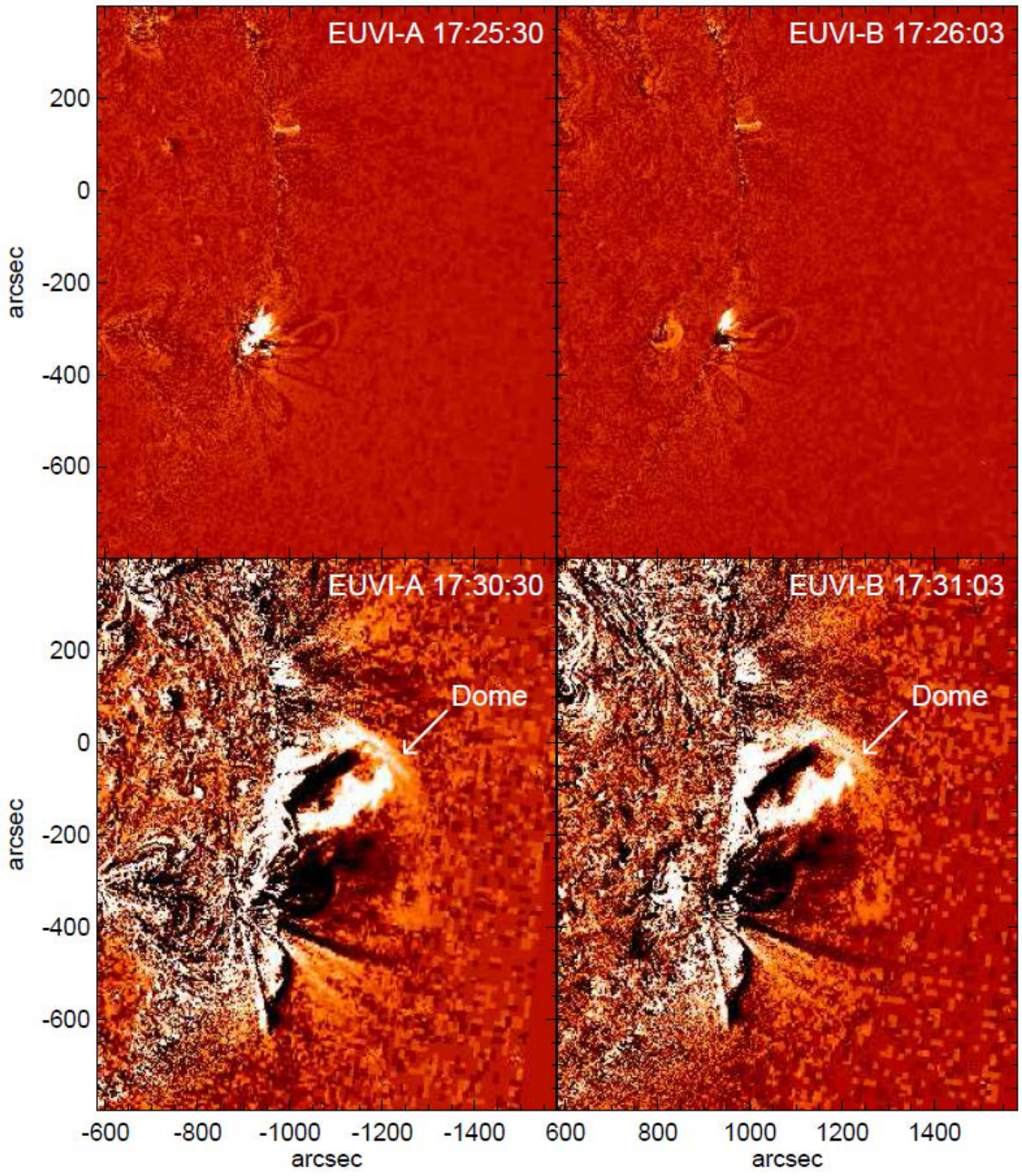


Fig. 4.— STEREO A (left panels) and B (right panels) EUVI observations of the disturbance on the limb at 17:25/17:26 UT (upper row) and 17:30/17:31 UT (lower row).

In Fig. 4, the STEREO–A images have been flipped east–west for easier comparison with the STEREO–B images, and the images have been scaled to put the satellites at Earth's distance from the Sun. The images are differenced with preflare images at 17:20/17:21 UT, several minutes before the flare. A much narrower range of brightness is displayed in the bottom panels in order to emphasize the faint outer emission. STEREO A was 87.1° ahead of the Sun–Earth line and STEREO B was 93.7° behind the Sun–Earth line at the time of the flare. The flare centroid is about 70″ ahead (west) of the Sun–Earth line. The coordinates in this perspective do not quite match those of the AIA images in Fig. 1 since the orientation of the solar rotation axis seen from STEREO is different than from the Earth perspective.

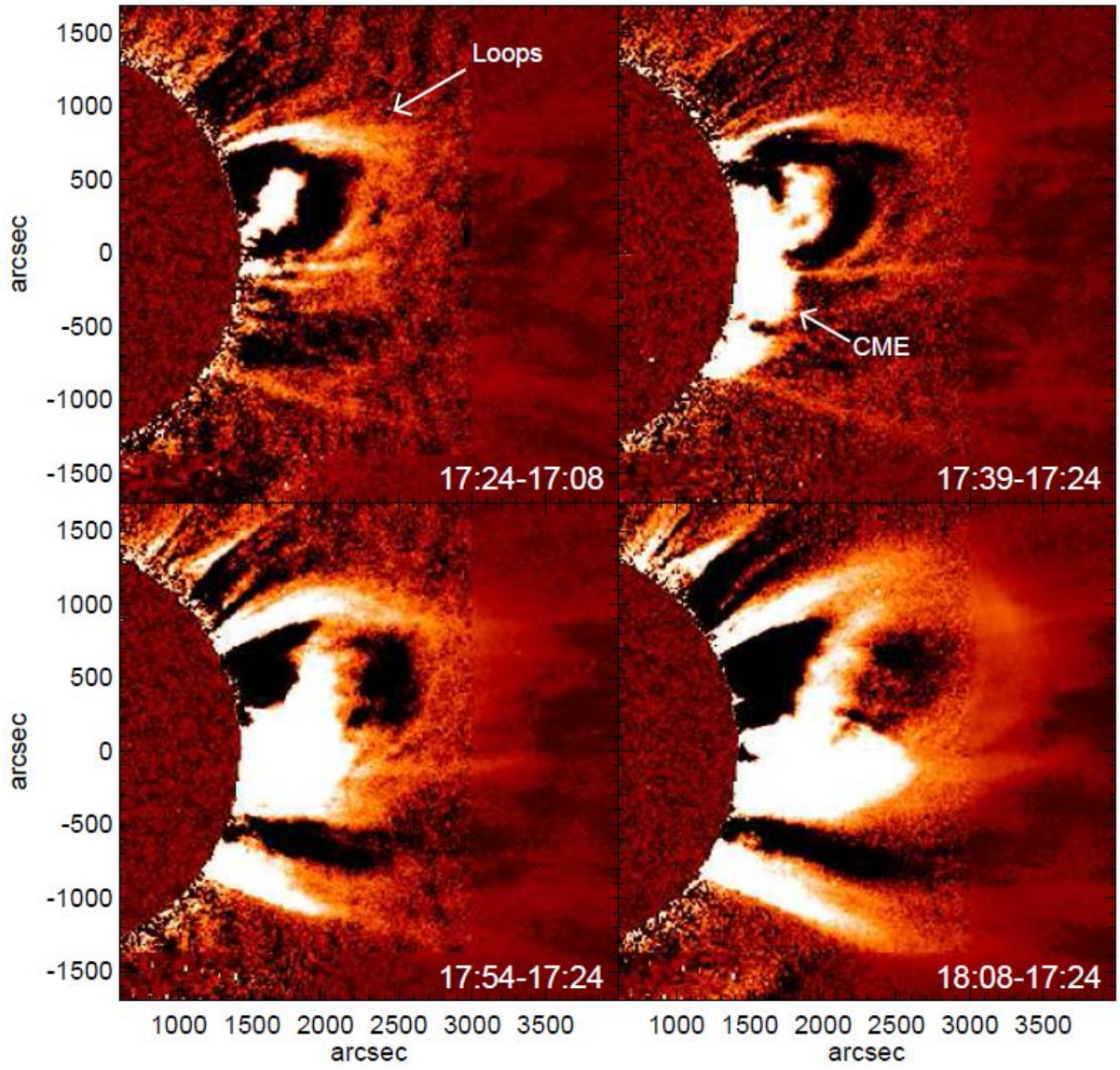


Fig. 5.— A sequence of SECCHI coronagraph images of the eruption at the limb.

In Fig. 5, COR1 images have been embedded within COR2 images to extend the radial height. We used flipped COR2-A images due to the fact that COR2-B images are occulted further out from the limb in the region of interest, but embedded with COR1-B images which have higher cadence than COR1-A. The top left panel shows the difference of two images prior to the eruption, and a loop system north of the equator is clearly seen to be expanding. The subsequent panels show differences with the last pre-eruption image: in the first (top right panel), the eruption from the flare is clearly visible just above the occulting disk in COR1, centered just south of the equator. In the subsequent images the two features cannot easily be separated.

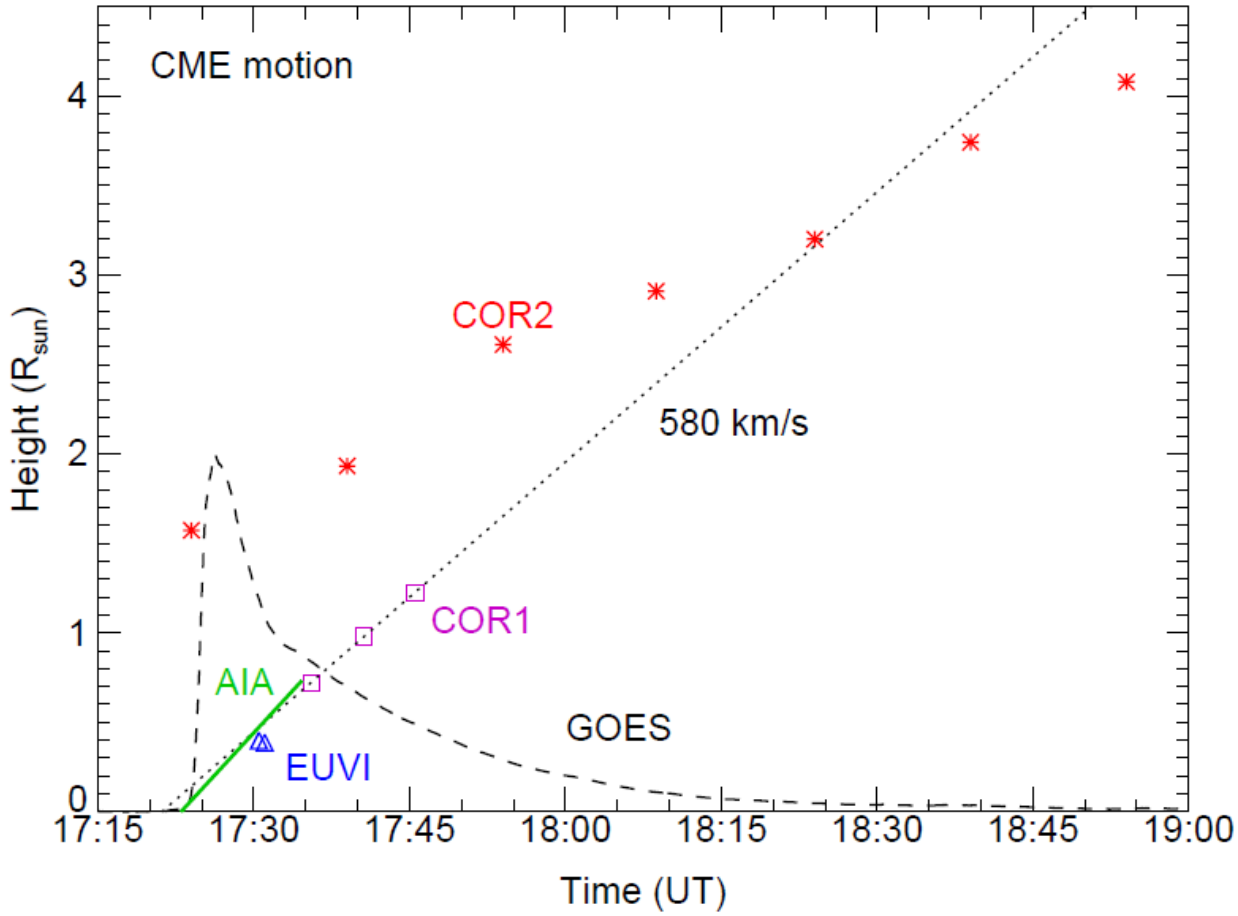


Fig. 6.— A plot of the distance of the leading edge of features visible in images of the eruption as a function of time.

In Fig. 6, the heights are all radial distances, except for the AIA plot. The EUVI heights come from the upper edge of the dome visible in Fig. 4. The COR1 points come from three COR1-A images with a cadence of 5 minutes. The COR2 points represent the maximum height of the merged feature consisting of the loops north of the equator and the CME from the flare: they are not simply separated in the COR2 images. The dashed line is a fit to the COR1 points, with a radial speed of 580 km $s^{-1}$; the green line represents the 730 km $s^{-1}$ motion of the EUV wave in the AIA data, which is presumably a lateral motion just above the visible surface rather than a radial motion.

## DISTRIBUTION LIST

DTIC/OCP
8725 John J. Kingman Rd, Suite 0944
Ft Belvoir, VA 22060-6218 1 cy

AFRL/RVIL
Kirtland AFB, NM 87117-5776 2 cys

Official Record Copy
AFRL/RVBXS/Edward W. Cliver 1 cy